PAPER

Emergence of novel hydrogen chlorides under high pressure†

Qingfeng Zeng,*[ab] Shuyin Yu,[ab] Duan Li,[ab] Artem R. Oganov[bcd] and Gilles Frapper[e]

HCl is a textbook example of a polar covalent molecule, and has a wide range of industrial applications. Inspired by the discovery of unexpected stable sodium and potassium chlorides, we performed systematic *ab initio* evolutionary searches for all stable compounds in the H–Cl system at pressures up to 400 GPa. Besides HCl, four new stoichiometries (H_2Cl, H_3Cl, H_5Cl and H_4Cl_7) are found to be stable under pressure. Our predictions substantially differ from previous theoretical studies. We evidence a high significance of zero-point energy in determining phase stability. The newly discovered compounds display a rich variety of chemical bonding characteristics. At ambient pressure, H_2, Cl_2 and HCl molecular crystals are formed by weak intermolecular van der Waals interactions, and adjacent HCl molecules connect with each other to form asymmetric zigzag chains, which become symmetric under high pressure. In H_5Cl, triangular H_3^+ cations are stabilized by electrostatic interactions with the anionic chloride network. Further increase of pressure drives H_2 dimers to combine with H_3^+ cations to form H_5^+ units. We also found chlorine-based Kagomé layers which are intercalated with zigzag HCl chains in H_4Cl_7. These findings could help to understand how varied bonding features can co-exist and evolve in one compound under extreme conditions.

1 Introduction

In 1935, Wigner proposed an insulator-to-metal transition in solid hydrogen under pressure.[1] The dissociation, rebonding and polymeriztion, and eventual metallization of molecular systems under high pressure provide a rich ground for novel physical and chemical phenomena. Chemical bonding is the key to understanding the structures and properties of materials, and impacts a broad range of fields including physics, chemistry, biology, and materials and planetary sciences. It is known that very unusual and unexpected compounds can become stable under pressure, accompanied by a variety of bizarre topologies, and their chemical nature is still not understood.[2,3] For example, under pressure, the simple Na–Cl system contains stable

compounds such as Na_3Cl, Na_2Cl, Na_3Cl_2, Na_4Cl_3, $NaCl_3$ and $NaCl_7$, as well as 'normal' NaCl.[4,5]

While NaCl is a textbook example of an ionic crystal, HCl is an archetypal polar covalent molecule. One can expect large differences between the Na–Cl and H–Cl systems; however, we can imagine the H–Cl system to be even more diverse due to its increased variety of intermolecular and intramolecular interactions. In addition, hydrogen adds extra excitement: the high-pressure metallic phase of hydrogen has been predicted to possess a nearly room-temperature superconductivity ($T_c \sim 240$ K),[6] while superconducting metallic hydrogen remains elusive. In 2014, an unusual stoichiometry, H_3S, was predicted with a high-T_c reaching ~ 200 K at 200 GPa.[7] Later, Eremets *et al.* verified that the phase responsible for high-T_c superconductivity (203 K) in the sulfur hydride system is H_3S.[8] It has been suggested that alloying hydrogen with other elements can greatly reduce the pressure required for stability of the superconducting state,[9] and one may think not of only metal hydrides, but also of compounds with more electronegative atoms, such as the aforementioned H_3S, or the H_nCl compounds studied here.

For the H–Cl system, HCl has been extensively studied in the past few decades.[10–13] At very low temperatures, HCl adopts an ordered orthorhombic $Cmc2_1$ structure, which is also adopted by HBr and HF.[11] With increasing pressure, the $Cmc2_1$ phase was suggested to transform into another orthorhombic $Cmcm$ structure at 51 GPa with hydrogen bond symmetrization.[14] The $Cmcm$ phase is stable until 108 GPa,[11] then a post-$Cmcm$ phase

[a] *Science and Technology on Thermostructural Composite Materials Laboratory, School of Materials Science and Engineering, Northwestern Polytechnical University, Xi'an, Shaanxi 710072, P. R. China. E-mail: qfzeng@nwpu.edu.cn*

[b] *International Center for Materials Discovery, School of Materials Science and Engineering, Northwestern Polytechnical University, Xi'an, Shaanxi 710072, P. R. China*

[c] *Department of Geosciences, Center for Materials by Design, and Institute for Advanced Computational Science, State University of New York, Stony Brook, NY 11794-2100, USA*

[d] *Moscow Institute of Physics and Technology, Dolgoprudny, Moscow Region 141700, Russia*

[e] *IC2MP UMR 7285, Université de Poitiers, CNRS, 4, rue Michel Brunet, TSA 51106, 86073 Poitiers Cedex 9, France*

† Electronic supplementary information (ESI) available. See DOI: 10.1039/c6cp08708f

with space group $P\bar{1}$ appears. However, at pressures higher than 230 GPa, the stability of HCl remains controversial. Duan et al.[15] predicted that the $P2_1/m$ structure would be the most stable one for HCl above 233 GPa, while a recent work by Chen et al.[12] proposed $C2/m$ and $P4/nmm$ structures, which are more stable than $P2_1/m$ above 250 GPa. Furthermore, the calculated enthalpy difference between $C2/m$ and $P4/nmm$ phases was negligibly small above 250 GPa. However, we know that zero-point energy (ZPE) usually plays a non-negligible role in the total energy of low-atomic-mass materials, and this effect was not considered in previous studies of the H–Cl system.

Besides HCl, several H_xCl_y compounds have also been predicted.[15,16] In 2015, Wang et al.[16] studied the crystal structures and phase stabilities of the hydrogen-rich H_2–HCl system by using a first-principles particle-swarm CALYPSO code. Between 100–300 GPa, two stable compounds with H_5Cl and H_2Cl stoichiometries were found. In H_5Cl, they found the stabilization of cationic H_3^+ species. It becomes almost an equilateral triangle under very high pressure. Soon after, Duan et al.[17] reexamined the phase stabilities of the H_2–HCl system by using the same CALYPSO code. However, very different results were found in their study. Besides H_5Cl and H_2Cl, Duan et al. found that H_3Cl and H_7Cl could also be stabilized in the pressure range of 0–250 GPa, which is in contradiction with the results of Wang et al.,[16] in which they found the very same two stoichiometries to be metastable up to 300 GPa. In the above two studies, their reactants are H_2 and HCl, thus the stabilities of the chlorine-rich phases in the full H–Cl system are still unclear. The question of whether a chlorine-rich structure can be stabilized under high pressure is still unresolved. Here, we apply a powerful evolutionary algorithm, USPEX, to extensively explore the crystal structures and stoichiometries in the H–Cl system. We attempt to give an exhaustive picture of the H–Cl system under pressure.

2 Methods

Searches for stable compounds in the H–Cl system from ambient pressure up to 400 GPa were performed using the variable-composition ab initio evolutionary algorithm USPEX.[18–20] In these searches, all H_xCl_y compositions were allowed, under the constraint that the total number of atoms in the primitive cell could be up to 30 atoms. The first generation contained 100 candidate structures, while all subsequent generations contained 80 structures. In each new generation, 40% of the structures were produced by heredity, 20% by softmutation, 20% by transmutation and 20% were produced randomly.

Local geometry relaxations were performed using density functional theory calculations with the use of VASP code.[21] These calculations are based on the Perdew–Burke–Ernzerhof (PBE) functional,[22] which belongs to the generalized gradient approximation (GGA) level of theory. We used the all-electron projector-augmented wave (PAW) method,[23,24] with the outermost core radius of 1.1 a.u. for the H atom and 1.9 a.u. for the Cl atom. The plane-wave kinetic energy cutoff was set to 900 eV, and uniform Γ-centered k-meshes with a reciprocal space resolution of $2\pi \times 0.03$ Å^{-1} were used for sampling the Brillouin zone. These settings enabled excellent convergence of the energy differences, stress tensors, and structural parameters. Phonon spectra were calculated using the finite-displacement method as implemented in the PHONOPY package[25] in order to probe the dynamical stability and explore the effects of ZPE on the thermodynamic stability of H_xCl_y compounds (see the ESI†).

All molecular species were optimized at different levels of theory (B3PW91, PBE, MP2, CCSD). A triple-zeta basis set was employed for all atoms, which was increased using both polarized and diffuse functions, aug-cc-pVTZ.[26,27] For each structure, the analytic Hessian was calculated to obtain the vibrational frequencies and determine the nature of the stationary point. These calculations were performed using the Gaussian package.[28] As the results followed the same trend, we present here only the electrostatic potential results based on the B3PW91 functional. The surface potentials, $V_s(r)$, were obtained using the Wave Function Analysis-Surface Analysis Suite (WFA).[29]

3 Results and discussion

The calculated convex hulls and pressure–composition phase diagram taking into account the vibrational contributions (ZPE) of the H–Cl system are shown in Fig. 1. The enthalpies of formation of the H_xCl_y phases have been calculated with respect to elemental hydrogen and chlorine in their most stable forms, i.e., $P6_3/m$, $C2/c$, $Cmca\bar{1}2$, $Cmca$ and $I4_1/amd$ structures for hydrogen,[30] and $Cmca$, $Fmm2$, $Immm$ and fcc structures for chlorine[31] in their stability fields. The convex hull is a set of thermodynamically stable states, which are stable with respect to disproportion into other phases or pure elements. Any structure, for which the enthalpy of formation lies on the convex hull, is considered to be thermodynamically stable and in principle can be synthesized from any isochemical mixture.

Besides reproducing the well-known HCl, we also found the stable stoichiometries 5:1, 3:1, 2:1 and 4:7. It can be seen
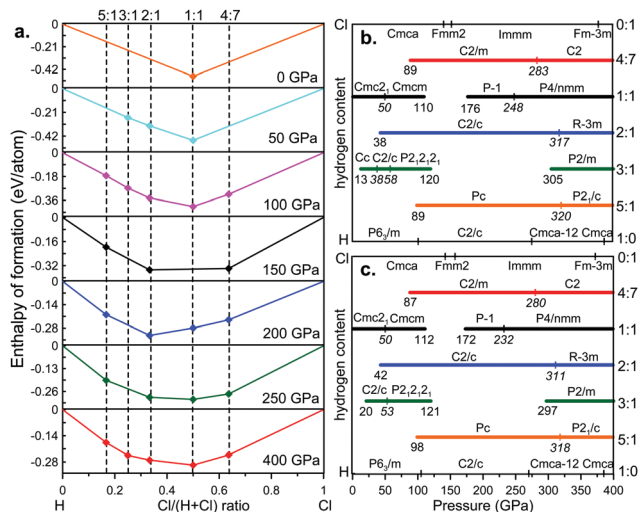

Fig. 1 (a) The calculated convex hulls of the H–Cl system at selected pressures. (b and c) Pressure–composition phase diagram of the H–Cl system between 0 and 400 GPa without (b) and with (c) ZPE corrections.

This journal is © the Owner Societies 2017

Phys. Chem. Chem. Phys., 2017, **19**, 8236–8242 | 8237

that HCl remains a stable compound in the pressure ranges of 0–112 GPa and 172–400 GPa, but between them, it will decompose into H_2Cl and H_4Cl_7. HCl is predicted to adopt four phases with the space groups $Cmc2_1$ (0–50 GPa), $Cmcm$ (50–112 GPa), $P\bar{1}$ (172–232 GPa) and $P4/nmm$ (232–400 GPa). For the low-pressure $Cmc2_1$ and $Cmcm$ phases, their enthalpies are indistinguishable above 50 GPa, due to the very similar structures. However, we find that hydrogen bond symmetrization occurs at around 50 GPa, consistent with previous studies.[11,12,16,17] After considering ZPE correction, the $P\bar{1}$ phase transforms into the $P4/nmm$ phase at 232 GPa instead of 250 GPa[12] proposed by Chen *et al.*[12] Besides, the $P4/nmm$ phase has a slightly lower enthalpy than the $C2/m$ structure.[12]

For H_7Cl discovered in the work of Duan *et al.*[17] (see Fig. S2, ESI†), we found it is metastable with or without considering the ZPE correction. For H_5Cl, our evolutionary searches revealed a new structure with the space group Pc at low pressures, which has a slightly lower energy than the previously proposed Cc structure[16,17] ($\sim$6 meV per atom at 150 GPa). At 318 GPa, the Pc phase transforms into a new structure with the space group $P2_1/c$. For H_3Cl, it emerges on the phase diagram at 20 GPa and decomposes into H_2Cl and H_5Cl at 121 GPa and reappears at 297 GPa, which is consistent with the results of Duan *et al.*[17] In their work, three phases with space groups Cc (12–40 GPa), $C2/c$ (40–60 GPa), and $P2_12_12_1$ (60–120 GPa)[17] were predicted (see Fig. S2, ESI†). However, when ZPE is taken into account, the $C2/c$ structure has a lower energy ($\sim$7 meV per atom at 25 GPa) and becomes more stable than the Cc structure. The transition pressure from $C2/c$ to $P2_12_12_1$ becomes 53 GPa instead of 60 GPa. For H_2Cl, the monoclinic $C2/c$ structure appears at 42 GPa and transforms to the highly-symmetric $R\bar{3}m$ structure at 311 GPa. Remarkably, we found a new chlorine-rich compound H_4Cl_7, which becomes stable at 87 GPa and remains stable up to 400 GPa.

Detailed lattice parameters and atomic Wyckoff positions of these thermodynamically stable H_xCl_y phases are given in Table S1 (ESI†). Their calculated phonon spectra displayed in Fig. S3 (ESI†) confirm that all these compounds are dynamically stable with no imaginary phonon modes in the whole Brillouin zone. After analyzing their crystal structures, we identified a rich variety of structural features, such as asymmetric or symmetric zigzag HCl chains, host–guest inclusion compounds, chlorine-based Kagomé layers, hcp chlorine network with interstitial protons and stretched H_2 units, one-dimensional (1D) hydrogen chains, bridging H_3^+ and H_5^+ units, interpenetrating graphene-like chlorine nets and others, which will be illustrated below.

3.1 HCl: a brief revisit of the pressure-induced symmetrization of the zigzag chains

At ambient conditions, HCl adopts the orthorhombic $Cmc2_1$ structure, which remains stable up to 50 GPa (Fig. 2a). In this structure, HCl forms zigzag chains with a H–Cl distance of 1.313 Å, compared with the calculated H–Cl bond length of 1.311 Å in the gas phase (exp. 1.274 Å). The intermolecular H–Cl separations in $Cmc2_1$ are 2.219 Å, much less than the sum of the van der Waals radii of 2.950 Å[32] and typical of H···Cl
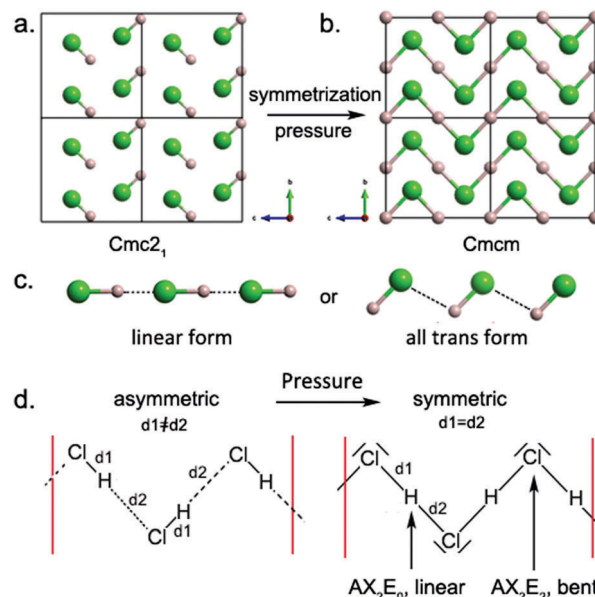

Fig. 2 (a and b) Crystal structures of $Cmc2_1$- and $Cmcm$-HCl. The big green spheres represent Cl atoms, while the small pink ones denote H atoms. (c) 1D planar HCl chain in linear and all-*trans* forms. (d) Lewis structure for the 1D symmetrized zigzag chain with VSEPR AX_nE_m notation.

hydrogen bonds. In the next $Cmcm$ phase, HCl···HCl contacts have an L-shaped geometry, with the H–Cl bond axis of one molecule perpendicular to the other one. A similar herringbone pattern is also observed in solid X_2 (X, halogen).[33,34] Why does the HCl chain possesses a zigzag shape (L-shaped geometry) rather than a linear or all-*trans* one (Fig. 2c)? Electrostatic arguments can be used to find the answer (Fig. 3).

The computed electrostatic potential $V_s(r)$ on the 0.001 a.u. surface of HCl is displayed in Fig. 3. A region of positive electrostatic potential – the so-called σ-hole[35,36] – can be seen on the outer surface of the hydrogen, with a maximum positive $V_{s,max}$ value of 44.6 kcal mol^{-1}. Due to the two chlorine lone pairs of electrons in the $3p_x$ and $3p_y$ orbitals, the most negative values $V_{s,min}$ are on the lateral rings of the chlorine negative potential surface, shown in red with a $V_{s,max}$ of -9.5 kcal mol^{-1}. Thus, the hydrogen atom may be considered as a Lewis acid site,

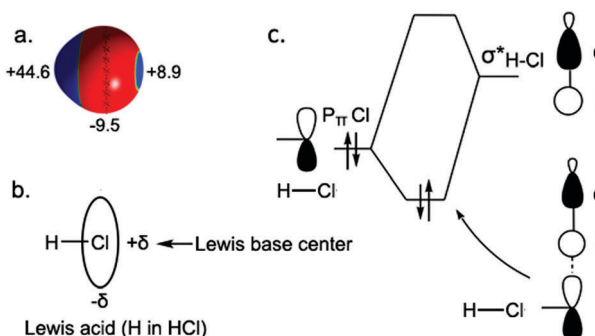
Fig. 3 (a) The computed electrostatic potential on the molecular surface of a HCl dimer. (b) Schematic σ-hole concept for hydrogen and halogen bonds. (c) Orbital interaction diagram of HCl···HCl dimer in an L-shaped coordination.

8238 | *Phys. Chem. Chem. Phys.*, 2017, **19**, 8236–8242

This journal is © the Owner Societies 2017

and the halogen atom interacts as an electron donor through its π lone pairs, thus the angle for the H⋯Cl–H arrangement should be around 90°, therefore the linear form is rejected. Moreover, to understand why the L-shaped coordination (Cl⋯H–Cl = 180°) is preferred to the all-*trans* one (Cl⋯H–Cl = 90°), molecular orbital arguments can be used. As depicted in Fig. 3c, the bonding interaction between the filled p_{π}(Cl) orbital – a lone pair of Cl – of an HCl unit and the vacant σ_{H-Cl}^{*} level of the other is optimized when the Cl⋯H–Cl angle is 180° (Fig. 3c). This two-electron stabilizing interaction and the anisotropy of the electron charge distribution of the halogen (Cl) atom explain why the HCl chain possesses an L-shaped geometry.

To summarize, this zigzag topology is closely related to the anisotropy of the electron charge distribution of the halogen (Cl) atom. A stabilizing interaction between two H–Cl units occurs in such a manner that a filled $Cl-p_{\pi}$ orbital – a π lone pair of Cl – is oriented towards the H–Cl bond of the other. Eventually, symmetric hydrogen bonds appear. These symmetric HCl-based zigzag chains are also encountered in other phases at different compositions.[11,14,37] In the *Cmcm* phase at 100 GPa, symmetric zigzag chains are stacked along the *a*-axis with an interchain spacing of 1.940 Å and a shortest Cl–Cl separation of 2.883 Å. Delocalized three-center two-electron bonding is expected along the σ H–Cl chains, which explains the increase in the covalent H–Cl bond length from 1.313 Å at 0 GPa to 1.442 Å at 100 GPa, and the decrease in the hydrogen-bond separation to 2.219 Å at 0 GPa. In agreement with the VSEPR model, here the zigzag chain contains chlorine atoms in a bent two-coordinate configuration (H–Cl–H angle of 84.2°) and two-coordinate almost linear hydrogen atoms (Fig. 2d and Fig. S4, ESI†).

The hydrogen bond symmetrization/desymmetrization process for HCl chains under high pressure is well characterized,[38] and can be considered as a classical example of a second-order Peierls distortion in weakly 1D covalent dimer-based chains. The symmetric zigzag HCl chain displays Peierls-type instability of the σ-bands at the Fermi level, which induces a structural distortion along the σ H–Cl backbone – creation of short and long H–Cl bonds – when the pressure is reduced to ambient conditions. This dimerization process leads to the thermodynamically stable covalent HCl monomers. Finally, in addition to hydrogen bond symmetrization, reduction of the van der Waals volume occurs under compression, leading to stronger interchain Cl–Cl interactions. From 0 to 100 GPa, the interplane π stacking separation decreases drastically from 3.506 Å to 1.940 Å, respectively, while the interplane σ stacking Cl–Cl separation decreases from 4.024 Å to 2.514 Å. This effect leads to band gap closure upon compression (Fig. S5, ESI†).

For the high-pressure HCl phases, our structure searches revealed the triclinic $P\bar{1}$ structure as the most stable one at 150 GPa. The $P\bar{1}$ structure contains four H–Cl molecules in the unit cell and only possesses the space-inversion symmetry. Note that the zigzag H–Cl chains discovered in the $Cmc2_1$ and *Cmcm* phases collapse in the $P\bar{1}$ phase instead of forming the intriguing distorted squares, where the chlorine atoms are connected by asymmetric hydrogen bonds. The tetragonal *P4/nmm* structure becomes stable at pressures above 232 GPa upon considering

the ZPE effect. *P4/nmm* HCl possesses a layered mackinawite-type structure, and adjacent HCl-based zigzag chains get close to form 2D layers. The shortest interlayer Cl–Cl distance is 2.199 Å at 300 GPa. In each layer, HCl zigzag chains run along the *a*- and *b*-axes. Here, hydrogen atoms have a distorted tetrahedral coordination (Cl–H–Cl angle of 126.7°), while chlorine atoms have a four-fold umbrella coordination, using the interlayer space to contain lone electron pairs. The increased H–Cl bond length reflects the increase in the number of H–Cl bonds under compression – four in *P4/nmm* (1.574 Å at 300 GPa), two in symmetric *Cmcm* HCl (1.442 Å at 100 GPa), one in molecular $Cmc2_1$ (1.313 Å at 0 GPa) – reflecting electron delocalization in the covalent 2D layers of the highest-pressure *P4/nmm* phase.

3.2 H_2Cl and H_3Cl: HCl zigzag chains + H_2 units

The hydrogen-rich compound H_2Cl crystallizes in the monoclinic *C2/c* structure (Fig. 4a). This structure is formed by planar symmetric zigzag HCl chains and H_2 dimers. H_2 dimers also form planar zigzag chains with alternating short intramolecular (0.733 Å at 100 GPa) and long intermolecular (1.563 Å at 100 GPa) distances. As expected from band theory (Peierls distortion), this encapsulated $(H_2)_n$ chain is insulating and presents yet another classical textbook hydrogen chain model in an experimentally synthesizable material. Pairs of stacked HCl chains are observed in the ac planes. A shortest Cl–Cl separation of 2.496 Å is found, compared to the van der Waals Cl–Cl separation of 3.50 Å at 0 GPa. Thus, some attractive interactions are at work in these paired chains, a signature of the chain-pairing effect.

At 311 GPa, the low-pressure *C2/c* structure transforms to a previously omitted[16] rhombohedral $R\bar{3}m$ structure (Fig. 4b), which has a cubic close packing of Cl atoms in which all octahedral voids are filled by H_2 groups. The H–H distance (1.057 Å) is much longer than that of the H_2 molecule (0.74 Å), though still bonding, which indicates weakening due to depletion of the σ-bonding orbital that donates part of its electron to the Cl framework. The band structure of the $R\bar{3}m$ phase displays a 'flat band-steep band' character[39] (Fig. S6, ESI†), suggesting potential superconductivity. The electron–phonon coupling (EPC) calculation shows that the EPC constant λ is 0.66 with an ω_{log} of 1368 K at 400 GPa. By using the Allen–Dynes modified McMillan equation,[40] we obtained the superconducting transition temperature (T_c) of 43.9–44.8 K ($\mu^* = 0.1$–0.13). Also, we found that coupling of the electrons to hydrogen vibrations in the frequency region of 33–60 THz contributes ~64.1% of the total λ.
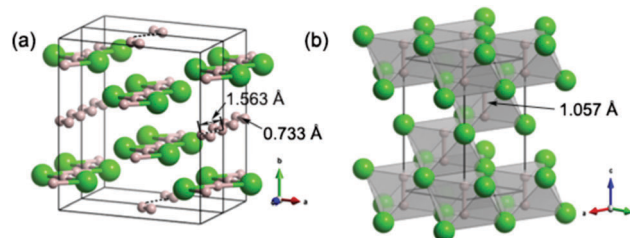

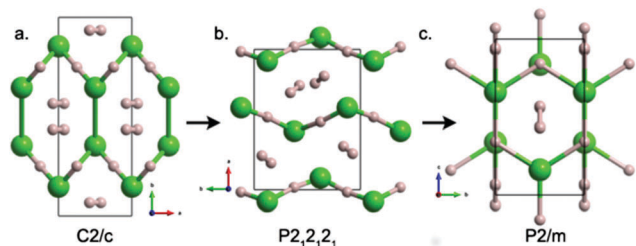Fig. 4 Crystal structures of H_2Cl in the (a) *C2/c* and (b) $R\bar{3}m$ phases.

This journal is © the Owner Societies 2017

Phys. Chem. Chem. Phys., 2017, **19**, 8236–8242 | 8239

Fig. 5 Crystal structures of H_3Cl in the (a) $C2/c$, (b) $P2_12_12_1$ and (c) $P2/m$ phases.

In $C2/c$-H_3Cl, the HCl units are also packed in symmetric zigzag chains, between which non-bonded H_2 molecules are located – formally two $(H_2Cl_2)_n$ polymers and four H_2 units per unit cell (Fig. 5a). The presence of H_2 reduces the pressure required to symmetrize H-bonds in the Cl–H–Cl chain in $Cmc2_1$-HCl. The $C2/c$ structure can be viewed as a host–guest inclusion compound: a stacked 1D planar inorganic polymeric HCl chain with encapsulated H_2 units in the van der Waals space. Symmetrization of the HCl chain occurs at ∼20 GPa, whereas in HCl it takes place at a much higher pressure of ∼50 GPa. Therefore, H_2 dimers act by either adding extra mechanical pressure or through chemical doping in the symmetrization process, lowering the driving force of the Peierls instability.

Obviously, free rotation is allowed around the bonding H–Cl chain, thus, a non-planar form may exist. In the higher-pressure $P2_12_12_1$ phase (Fig. 5b), slightly helical zigzag HCl chains run along the b-axis. The dihedral angle H–Cl–Cl–H is 14.1° at 100 GPa. There are four H_2 dimers per unit cell located in the cavities between two slightly helical chains. Above 271 GPa, a $P2/m$ structure is stable (Fig. 5c). One can observe graphene-like arrays formed together by Cl and H atoms, some parallel and some perpendicular to the ac plane. The graphene-like nets are composed by the staggered packing of symmetric HCl zigzag chains. H_2 units are observed in channels formed by graphene-like nets.

3.3 H_5Cl: the existence of H_3^+ and H_5^+ units

The crystal structures of H_5Cl phases are shown in Fig. 6. The low-pressure Pc structure contains planar chains composed of triangular H_3 units connected to two Cl atoms. The structure also contains isolated H_2 dimers (H–H = 0.748 Å at 150 GPa). Formally, the H_3 unit may be viewed as the well-known H_3^+ cation interacting with one Cl^- anion. The H_3^+ cation deviates slightly from an equilateral triangle (H–H = 0.864–0.913 Å at 150 GPa), which is the shape experimentally and theoretically observed in the gas phase H_3^+ for this smallest and simplest aromatic molecule.[41] The H–H bond lengths are elongated by 19% relative to the calculated distance in encapsulated H_2 dimers or the experimental free gas H_2 (0.74 Å). Such elongation is expected for an electron-deficient system (Fig. 6c). The stability of H_3^+ can be attributed to the occupation of the a_1' bonding molecular orbital (MO) and the large HOMO a_1'-LUMO e' gap. The formal H–H bond order is 1/3 per H–H link (1 in H_2), explaining the longer H–H distances for H_3^+ (H_3^+ can be described by the well-known three-center two-electron bonding

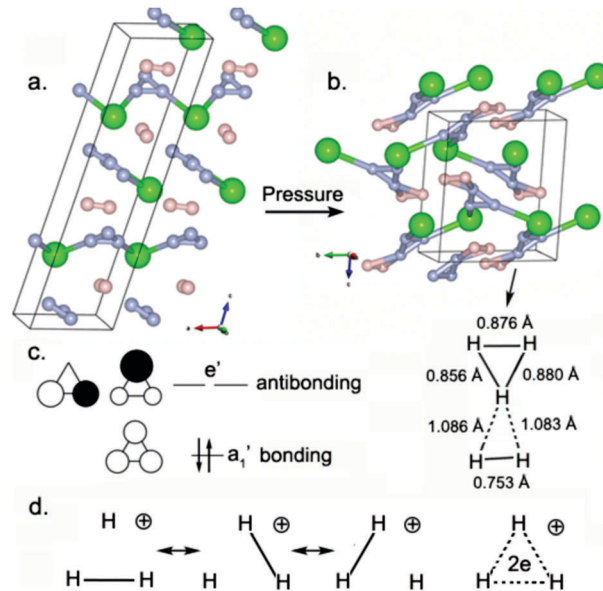Fig. 6 Crystal structures of H_5Cl in the (a) Pc phase at 150 GPa and (b) $P2_1/c$ phase at 350 GPa. (c and d) Molecular orbital diagram and Lewis structures for the H_3^+ cation.

scheme). H_3^+ is stabilized in this solid-state compound by electrostatic interactions with the anionic chloride network.

H_2 acts as an electron donor in combination with a proton to yield H_3^+. By analogy, H_2 may also combine with H_3^+, leading to the higher homolog H_5^+ (Fig. S7, ESI†). The existence of H_3^+ and H_5^+ has been firmly established by mass spectrometry and quantum-mechanical calculations.[41–44] In fact, gas phase charged hydrogen clusters are a well-known stable species, provided that the number of hydrogen atoms is odd.[45,46] The H_5^+ ion appears in the high-pressure $P2_1/c$ phase of H_5Cl. The H–H distances reveal the existence of the planar H_5^+ unit: all H–H distances are in the range of 0.753–1.086 Å at 350 GPa. In the pseudo-equilateral H_3 unit, the H–H bond lengths are 0.856–0.880 Å. Two H–H bonds are significantly longer (1.083–1.086 Å) than the H–H bonds reported in H_3 units, indicating weaker bonds. The shortest distance is 0.753 Å, similar to the length of the H–H covalent bond in free H_2 gas. Therefore, this planar H_5 unit may be viewed as H_3^+ interacting with a slightly activated H_2 dimer. A five-center four-electron bonding scheme is assigned: such a bonding mode has been previously observed in protonated hydrogen-based clusters,[47] the global-minimum structure of which is, however, non-planar. The calculated electronic properties show that this compound is an insulator up to 400 GPa (Fig. S5, ESI†). Obviously, a hydrogen-rich system is not more easily metallized than a chlorine-rich system.

3.4 H_4Cl_7: chlorine-based Kagomé layers intercalated with zigzag HCl chains

Besides H-rich H_xCl_y compounds, we also uncovered a Cl-rich compound H_4Cl_7, which has never been reported before. H_4Cl_7 has two structures in the pressure range 0–400 GPa, i.e. $C2/m$ (87–280 GPa) and $C2$ (280–400 GPa). In the low-pressure $C2/m$

8240 | Phys. Chem. Chem. Phys., 2017, 19, 8236–8242

This journal is © the Owner Societies 2017

phase (Fig. 7a), two different networks can be found, namely two $(HCl)_2$ zigzag chains intercalated between planar Kagomé $(Cl_3)_2$ covalent layers $(4H_2Cl_2 + 2Cl_3 = H_8Cl_{14})$. The 1D zigzag chain has the topology encountered in the $Cmcm$-HCl phase with two-coordinate bent chlorine atoms and two-coordinate (almost) linear hydrogens (Cl–H = 1.46–1.47 Å; H–Cl–H = 98.7°; Cl–H–Cl = 173.5°). Besides, the $C2/m$ structure contains a 2D hexagonal network of chlorine atoms comprising triangles and hexagons, shown in Fig. 7b. The planar Kagomé $(Cl_3)_2$ covalent layers possess four-coordinate (with rectangular planar coordination) chlorine atoms with Cl–Cl bond distances of 2.236–2.273 Å and bond angles of 60.5° and 119.5° at 100 GPa. Seven electrons may be formally assigned to each chlorine atom, thus according to the VSEPR model, the chlorine atom is the $AX_4E_{3/2}$ type, a rectangular planar AX_4 unit (one electron less than that of XeF_4[48]).

The high-pressure $C2$ phase has even more complex substructures (Fig. 8a). First, the 2D Kagomé chlorine (3636) layers found in the low-pressure $C2/m$ phase still exist (Cl–Cl = 2.146–2.162 Å at 350 GPa). Second, between these planar Kagomé layers, there are two zigzag $(HCl)_2$ chains with two types of coordinated chlorine atoms: one is coordinated to two bridging hydrogen atoms (H–Cl = 1.367–1.387 Å), the other is four-coordinated to two bridging hydrogen atoms (H–Cl = 1.375–1.379 Å) and two chlorine atoms through short and long bonds (Cl–Cl = 2.051–2.223 Å). Finally, one may see 1D linear chlorine chains running through the center of Cl_6 hexagons

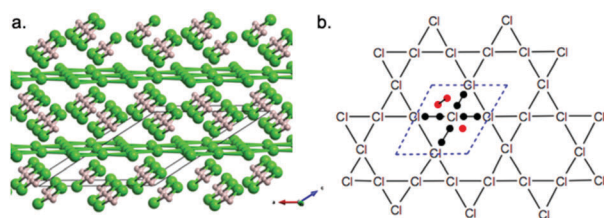**Fig. 7** (a) Crystal structure of $C2/m$-H_4Cl_7 at 100 GPa. (b) VSEPR analysis of the planar Kagomé $(Cl_3)_2$ covalent layers.

with alternating distances (2.006 Å and 2.183 Å). Even though this phase displays delocalized bonding (*e.g.* the Cl–Cl long distance of 2.223 Å, signature of an electron-deficient covalent bond), its local structures are rationalized by using VSEPR rules from single Lewis resonant structures (Fig. 8b and Fig. S8, ESI†). For the 1D zigzag $(HCl)_2$ chains, the two-coordinate chlorine atoms are AX_2E_2 type with a bent geometry (H–Cl–H = 99.2°). The four-coordinate chlorine atoms are AX_4E_1 type with a local butterfly-like structure (H–Cl–H = 92.3°, Cl–Cl–Cl = 172.4°). The two-coordinate hydrogen atom is AX_2E_0 type with a (almost) linear geometry. DFT calculations show that both $C2/m$- and $C2$-H_4Cl_7 phases are metallic, mainly due to the Cl-p states.

4 Conclusion

In summary, we have extensively explored the stable stoichiometries and structures in the H–Cl system up to 400 GPa. Besides HCl, we also discovered three hydrogen-rich compounds, H_2Cl, H_3Cl and H_5Cl, and a chlorine-rich compound H_4Cl_7. HCl and H_3Cl show reentrant behavior. With increasing pressure, they will first decompose into adjacent stoichiometries, then become stable at a higher pressure again. Our results show that the ZPE contribution to the total energy will significantly affect the stability of H_xCl_y compounds. After considering ZPE corrections, $P4/nmm$-HCl has lower enthalpy than the previously proposed $C2/m$ structure, and $C2/c$-H_3Cl has a lower enthalpy than the Cc structure proposed by Duan *et al.* Besides, we found a Pc structure for H_5Cl at low pressures, which is more energetically favorable than the Cc structure. And H_7Cl is metastable with or without ZPE correction in the whole studied pressure range.

The newly discovered H_xCl_y compounds possess peculiar structural characteristics and rich chemical bonding types. Here, we used VSEPR and molecular orbital theory to rationalize their formation. The zigzag shape of H–Cl···H–Cl chains can be explained by the Lewis acid model based on electrostatic potential calculations. Under high pressure, asymmetric zigzag chains become symmetric. In H_5Cl, triangular H_3^+ cations are stabilized by electrostatic interactions with the anionic chloride network. Further increase of pressure makes H_2 dimers combine with H_3^+ cations to form H_5^+ units. Additionally, we found chlorine-based Kagomé layers in H_4Cl_7, intercalated with zigzag HCl chains. These findings of unexpected complexity in the simple H–Cl system will be helpful in understanding the effect of pressure on chemical bonding.
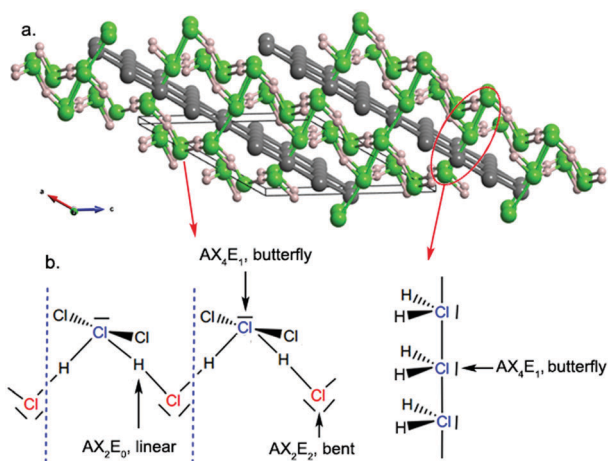
Acknowledgements

Fig. 8 (a) Crystal structure of $C2$-H_4Cl_7 at 350 GPa. The chlorine-based Kagomé layers are drawn in grey color. (b) VSEPR analyses of the zigzag HCl chain (left) and the linear chlorine one (right) in the $C2$ phase.

This journal is © the Owner Societies 2017

Phys. Chem. Chem. Phys., 2017, **19**, 8236–8242 | **8241**

References

1 E. Wigner and H. B. Huntington, *J. Chem. Phys.*, 1935, **3**, 764–770.

2 W. Grochala, R. Hoffmann, J. Feng and N. W. Ashcroft, *Angew. Chem., Int. Ed.*, 2007, **46**, 3620.

3 E. Zurek and W. Grochala, *Phys. Chem. Chem. Phys.*, 2015, **17**, 2917–2934.

4 W. Zhang, A. R. Oganov, A. F. Goncharov, Q. Zhu, S. E. Boulfelfel, A. O. Lyakhov, E. Stavrou, M. Somayazulu, V. B. Prakapenka and Z. Konôpková, *Science*, 2012, **342**, 1502–1505.

5 G. Saleh and A. R. Oganov, *Phys. Chem. Chem. Phys.*, 2016, **18**, 2840–2849.

6 N. W. Ashcroft, *Phys. Rev. Lett.*, 1968, **21**, 1748–1749.

7 D. Duan, Y. Liu, F. Tian, D. Li, X. Huang, Z. Zhao, H. Yu, B. Liu, W. Tian and T. Cui, *Sci. Rep.*, 2014, **4**, 6968.

8 A. P. Drozdov, M. I. Eremets, I. A. Troyan, V. Ksenofontov and S. I. Shylin, *Nature*, 2015, **525**, 73–76.

9 N. W. Ashcroft, *Phys. Rev. Lett.*, 2004, **92**, 187002.

10 J. Obriot, F. Fondère, P. Marteau and M. Allavena, *J. Chem. Phys.*, 1983, **79**, 33–42.

11 L. Zhang, Y. Wang, X. Zhang and Y. Ma, *Phys. Rev. B: Condens. Matter Mater. Phys.*, 2010, **82**, 1558–1564.

12 C. Chen, Y. Xu, X. Sun and S. Wang, *J. Phys. Chem. C*, 2015, **119**, 17039–17043.

13 H. Shimizu, K. Kamabuchi, T. Kume and S. Sasaki, *Phys. Rev. B: Condens. Matter Mater. Phys.*, 1999, **59**, 11727–11732.

14 K. Aoki, E. Katoh, H. Yamawaki, M. Sakashita and H. Fujihisa, *Phys. B*, 1999, **265**, 83–86.

15 D. Duan, F. Tian, Z. He, X. Meng, L. Wang, C. Chen, X. Zhao, B. Liu and T. Cui, *J. Chem. Phys.*, 2010, **133**, 074507.

16 Z. Wang, H. Wang, J. S. Tse, T. Iitaka and Y. Ma, *Chem. Sci.*, 2014, **6**, 522–526.

17 D. Duan, X. Huang, F. Tian, Y. Liu, D. Li, H. Yu, B. Liu, W. Tian and T. Cui, *J. Phys. Chem. A*, 2015, **119**, 11059–11065.

18 A. R. Oganov and C. W. Glass, *J. Chem. Phys.*, 2006, **124**, 244704.

19 A. O. Lyakhov, A. R. Oganov, H. T. Stokes and Q. Zhu, *Comput. Phys. Commun.*, 2013, **184**, 1172–1182.

20 A. R. Oganov, A. O. Lyakhov and M. Valle, *Acc. Chem. Res.*, 2011, **44**, 227–237.

21 G. Kresse and J. Furthmüller, *Comput. Mater. Sci.*, 1996, **6**, 15–50.

22 J. P. Perdew, K. Burke and M. Ernzerhof, *Phys. Rev. Lett.*, 1996, **77**, 3865–3868.

23 P. E. Blöchl, *Phys. Rev. B: Condens. Matter Mater. Phys.*, 1994, **50**, 17953–17979.

24 G. Kresse and D. Joubert, *Phys. Rev. B: Condens. Matter Mater. Phys.*, 1999, **59**, 1758.

25 A. Togo, F. Oba and I. Tanaka, *Phys. Rev. B: Condens. Matter Mater. Phys.*, 2008, **78**, 134106.

26 R. A. Kendall, T. H. Dunning and R. J. Harrison, *J. Chem. Phys.*, 1992, **96**, 6796–6806.

27 E. R. Davidson, *Chem. Phys. Lett.*, 1996, **260**, 514–518.

28 M. J. Frisch, G. W. Trucks, H. B. Schlegel, G. E. Scuseria and M. A. Robb, *et al.*, *Gaussian*, 2001.

29 F. A. Bulat, A. Toro-Labbé, T. Brinck, J. S. Murray and P. Politzer, *J. Mol. Model.*, 2010, **16**, 1679–1691.

30 C. J. Pickard and R. J. Needs, *Nat. Phys.*, 2007, **3**, 473–476.

31 P. Li, G. Gao and Y. Ma, *J. Chem. Phys.*, 2012, **137**, 2840–2847.

32 A. Bondi, *J. Phys. Chem.*, 1964, **68**, 441–451.

33 G. Bao, D. Duan, D. Zhou, X. Jin, B. Liu and T. Cui, *J. Phys. Chem. B*, 2010, **114**, 13933–13939.

34 G. Bao, D. Duan, F. Tian, L. Wang, B. Liu and T. Cui, *J. Chem. Phys.*, 2011, **134**, 123–127.

35 T. Clark, M. Hennemann, J. S. Murray and P. Politzer, *J. Mol. Model.*, 2007, **13**, 291–296.

36 T. Clark, *Wiley Interdiscip. Rev.: Comput. Mol. Sci.*, 2013, **3**, 13–20.

37 Y. Duan and D. C. Sorescu, *J. Chem. Phys.*, 2010, **133**, 304–311.

38 P. Li, G. Gao and Y. Ma, *J. Chem. Phys.*, 2012, **137**, 2840–2847.

39 A. Simon, *Angew. Chem., Int. Ed. Engl.*, 1997, **36**, 1788–1806.

40 P. B. Allen and R. C. Dynes, *Phys. Rev. B: Solid State*, 1975, **12**, 905–922.

41 R. D. Poshusta and F. A. Matsen, *J. Chem. Phys.*, 1967, **47**, 4795–4799.

42 J. J. Thomson, *J. Rönt. Soc.*, 1922, **18**, 150–151.

43 R. E. Christoffersen, *J. Chem. Phys.*, 1964, **41**, 960–971.

44 P. H. Dawson and A. W. Tickner, *J. Chem. Phys.*, 1962, **37**, 672–673.

45 H. Chermette and I. Ymmud, *Phys. Rev. B: Condens. Matter Mater. Phys.*, 2001, **63**, 165427.

46 M. Farizon, B. Farizon-Mazuy, N. de Castro Faria and H. Chermette, *Chem. Phys. Lett.*, 1991, **177**, 451–457.

47 I. Štich, D. Marx, M. Parrinello and K. Terakura, *J. Chem. Phys.*, 1997, **107**, 9482–9492.

48 Q. Zhu, D. Y. Jung, A. R. Oganov, C. W. Glass, C. Gatti and A. O. Lyakhov, *Nat. Chem.*, 2013, **5**, 61–65.